

Lack of biochemical signalling in GelMA leads to polarity reversion in intestinal organoids independent from mechanoreciprocity

Journal of Tissue Engineering
Volume 16: 1–15
© The Author(s) 2025
Article reuse guidelines:
sagepub.com/journals-permissions
DOI: 10.1177/20417314251345000
journals.sagepub.com/home/tej



Lenie Vanhove^{1,2} , Thomas Van Gansbeke³, Bert Devriendt⁴,
Ruben Van der Meeren³, Ruslan I. Dmitriev¹ 
and Irina A. Okkelman¹ 

Abstract

Xenogeneic tumour origin and batch-to-batch variability of Engelbreth-Holm-Swarm sarcoma tumour cell-derived hydrogels (Matrigel, Cultrex) limit the biomedical application of organoids in tissue engineering. The gelatin-methacryloyl (GelMA) hydrogels represent a defined, tunable, and GMP-friendly alternative, but they are rarely studied as alternative to Matrigel. Here, we studied effects of mechanical properties of GelMA and addition of laminin-III on encapsulation and growth of small intestinal organoids. GelMA-embedded organoids displayed polarity reversion, resulting in apical-out and apical-basal phenotypes, independent from the matrix stiffness. Addition of laminin-III softened hydrogels and also resulted in a partial restoration of the basal-out phenotype. Interestingly, despite the incomplete polarity restoration, GelMA-organoids still showed minor growth. GelMA stiffness and concentration influenced the transition from 3D to 2D organoid cultures. Collectively, our study confirms that tuning of GelMA mechanical properties alone cannot recapitulate the basal membrane matrix. However, controlled polarity reversion offers a tool for engineering organoids and enabling apical membrane access.

Keywords

GelMA, intestinal organoids, polarity reversion, Matrigel, mechanoreciprocity

Received: 11 February 2025; accepted: 9 May 2025

Introduction

Within a human body, cells reside in a complex three-dimensional (3D) extracellular matrix (ECM), providing unique tissue-specific biochemical cues, crucial for structural support of stem and differentiating cells.¹ Its main components are structural proteins including collagen type I (e.g. the most abundant collagen type), elastin, and fibronectin, as well as polysaccharides and proteoglycans. The dynamics of ECM biochemical (macromolecules, small molecules, secretome, extracellular vesicles, ions, and other factors) and physical (anisotropic elasticity, viscosity, and stiffness) components influence cell behavior.^{1,2} One of the major tasks of tissue engineering (TE) is recapitulating ECM composition and properties in vitro

¹Tissue Engineering and Biomaterials Group, Department of Human Structure and Repair, Faculty of Medicine and Health Sciences, Ghent University, Belgium

²Mitochondrial Investigations Laboratory, Department of Internal Medicine and Pediatrics, Faculty of Medicine and Health Sciences, Ghent University, Belgium

³Rousselot BV, Darling Ingredients, Ghent, Belgium

⁴Laboratory of Immunology, Department of Translational Physiology, Infectiology and Public Health, Faculty of Veterinary Medicine, Ghent University, Merelbeke, Belgium

Corresponding author:

Ruslan I. Dmitriev, Tissue Engineering and Biomaterials Group, Department of Human Structure and Repair, Faculty of Medicine and Health Sciences, Ghent University, C. Heymanslaan 10, Ghent 9000, Belgium.

Email: Ruslan.Dmitriev@UGent.be



Creative Commons Non Commercial CC BY-NC: This article is distributed under the terms of the Creative Commons

Attribution-NonCommercial 4.0 License (<https://creativecommons.org/licenses/by-nc/4.0/>) which permits non-commercial use, reproduction and distribution of the work without further permission provided the original work is attributed as specified on the SAGE and Open Access pages (<https://us.sagepub.com/en-us/nam/open-access-at-sage>).

for subsequent 3D *in vitro* modelling, tissue mass production, or regenerative medicine applications.^{2,3}

The relevance of naturally derived ECM hydrogels is underscored by their broad application in stem cell-derived organoid models. Sato, Clevers and co-workers⁴ demonstrated that adult stem cells can self-organise and reconstruct a crypt-like functional organisation when grown in a Matrigel matrix, producing the ‘intestinal organoid’ model. Small intestinal organoids, which can be produced from adult and induced pluripotent stem cells (iPSC), can recapitulate *in vitro* and *ex vivo* various functional aspects of the intestinal epithelium, including nutrient absorption, barrier function, complex cell composition, and can be used as a model to study host-pathogen interactions, prompting their wider use in producing multi-tissue and multi-organ lab-on-a-chip models, tissue repair, and disease modelling.^{5,6} The success in generating small intestinal organoids sparked a growing interest in producing organoids from many other tissue types.⁷ Advanced models, based on organoids can represent assembloids, hybrid bioelectronics, organ-on-a-chip, or more complex structures, holding promise in potentially improved scalability and producing fully autologous tissue building blocks from the same donor.⁸

However, the most widely used hydrogel to culture organoids, iPSC, and cancer cells, Matrigel, is sourced from Engelbreth-Holm-Swarm (EHS) mouse sarcoma tumour cells.⁹ Matrigel provides cues of the basement membrane (BM), which are thin layers of a specialised ECM, essential for stem cell function and organoid production. It contains laminin, collagen IV, and different ECM proteins, important for growing and differentiating organoids. Depending on the concentration used within Matrigel, it has a Young’s Modulus of <math><0.5\text{--}1.5\text{ kPa}</math>, which is in the range of soft tissue and undergoes an inverse temperature transition, being liquid at 4°C and gel at 37°C.^{10–12} However, Matrigel and related EHS extracts are derived from mouse sarcoma tumour cells, making its use in human clinical applications impossible. Its manufacturing also involves challenging ethics (multiple mice are used to produce the extract, no compliance with the 3R principle) and leads to batch-to-batch variability and therefore poor compatibility with tuning mechanical properties. In addition, it is expensive, not fully defined (>1600 peptides and proteins with varying composition) and not compliant with GMP standards.^{13–16} Given all these limitations, developing refined and biocompatible semi-synthetic alternatives to Matrigel, represents one of the paramount tasks for organoids and tissue engineering.

To address the limitations of the Matrigel, several synthetic and semi-synthetic hydrogels have been proposed, based mostly on modified PEG and employing azide-alkyne and related ‘click’ chemistry approaches.^{17–19} These hydrogels aim at providing a defined microenvironment, mimicking the ECM, while avoiding the batch-to-batch variability seen in Matrigel. For instance, PEG-based

hydrogels supplemented with ECM peptides were proposed as prospective materials, supporting the growth and differentiation of intestinal organoids.²⁰ Gelatin methacryloyl (GelMA) hydrogels, first described by Van Den Bulcke et al.²¹ represents an appealing alternative to Matrigel, due to its photo-crosslinkable nature and cell biocompatibility. GelMA is now a popular semi-synthetic hydrogel, finding many applications in 3D cell culture and bioprinting.^{22,23} It consists of the natural polymer gelatin, derived from collagen, and modified with methacryloyl functional groups (MA).²¹ Photo-crosslinking is used to form a covalently bound network of MA groups, which results in a GelMA hydrogel.²⁴ The frequently used photoinitiator lithium acylphosphonate salt (LAP) has a high solubility in water and efficient light absorption at 365 nm, with minimal effects on cell viability, low immunogenicity, and biodegradability.^{25,26} GelMA also contains arginine-glycine-aspartate (RGD) sequences, supporting cell adhesion, proliferation, and differentiation.²⁷ The physical properties of GelMA can be defined by the degree of functionality (DoF), the Mw, the GelMA concentration, and the UV exposure time of GelMA. These variables allow fine-tuning of the physical properties and can influence viability, differentiation, and proliferation of cells and tissue encapsulated in GelMA hydrogels. A higher concentration is also correlated with a smaller pore size, influencing the migration of the cells or 3D cellular structures in the hydrogel.^{28–30}

To the best of our knowledge, reports on the application of GelMA in the culture of small intestinal organoids are lacking. A few recent studies applied GelMA to cell cultures of intestinal-like cells (Caco-2), as well as neural, liver and salivary gland organoids.^{31–33} Neuronal organoids embedded within GelMA facilitated the formation of functional neural networks. On the other hand, GelMA was used to mimic the ECM for liver organoids and seemed to improve the functional hepatic tissue and its metabolic activity.³¹ With salivary gland organoids, GelMA-based scaffolds also supported the growth and differentiation. In addition, collagen I-based matrices were successfully used for intestinal organoid culture,³⁴ which indicates that GelMA-based hydrogels, displaying tuneable mechanical properties and ease of production, represent promising materials for intestinal epithelium engineering. Here, we investigated how GelMA hydrogels with tuneable mechanoreciprocity supported small intestinal organoid growth, proliferation, and differentiation as compared to Matrigel.

Materials and methods

Materials

X-PURE® GelMA products (based on type A gelatin) were provided by Rousselot BV (Ghent, Belgium). The X-PURE® GelMA products 90p40, 90p60, 160p60, and

160p80, with a concentration of 5% and 10% were used. The products exhibit variations in both average molecular weight (Mw) and degree of functionality (DoF). Here, 90 and 160 are the Mw in kDa, 40, 60, and 80 are the DoF and p stands for porcine. Cell culture sterile plasticware was obtained from VWR (Belgium). For microscopy, organoids were transferred and grown onto microscopy dishes (coverglass no. 1.5 thickness, e.g. μ -slide 12-well, Ibidi GmbH, Germany, Cat. No. 80821).

Dyes

Calcein Green AM (Cat. No. AS-89201, Tebubio, France), Hoechst 33342 (Cat. No. H3570, Invitrogen, Belgium), propidium iodide (Cat. No. 25535-16-4, Sigma-Aldrich, Belgium), APN-specific VHH (clone 3L94)³⁵ fused with the Fc domain of mouse IgG2a, Goat anti-Mouse IgG (H + L) cross-preabsorbed secondary antibody, Alexa Fluor 488-conjugated (Cat. No. A-11001, Thermo Fisher Scientific Inc., Belgium) and phalloidin-Alexa Fluor 546 (Cat. No. A2228, Thermo Fisher Scientific Inc., Belgium).

Synthesis and characterisation of GelMA hydrogels

Different GelMA products were dissolved in $0.1 \times$ phosphate-buffered saline (PBS; Sigma-Aldrich, Cat. No. 818708) and placed in the oven ($+45^\circ\text{C}$, 2h). GelMA products were sterilised using double filtration through 0.45 and 0.2 μm filters (Thermo Fisher, Cat. No. 5640020) in the laminar airflow cabinet. For crosslinking, lithium phenyl-2,4,6-trimethyl-benzoylphosphinate (LAP; Sigma-Aldrich, Cat. No. 85073-19-04) was used, dissolved in $0.9 \times$ PBS. After freeze-drying of GelMA (7 days), the solid product was weighed and mixed with sterile LAP-PBS to reach a 5% and 10% GelMA concentration. After addition of the LAP-PBS to the freeze-dried products, the solution was vortexed (10–20s), incubated in a water bath ($+45^\circ\text{C}$) until complete dissolution and disappearance of foam. Each GelMA solution was made in triplicate in a dome formation (50 μL , ± 0.8 mm diameter and ± 1 mm thickness) within a 24 well-plate and cured by 365 nm UV light ($8 \text{ mW}/\text{cm}^2$, 30 s or 1 min). Mouse laminin-111 (Corning, Cat. No. 354232) was added to the 5% or 10% GelMA products, at a final concentration of 5 or 100 $\mu\text{g}/\text{mL}$. The resulting GelMA products were stored in the dark at $+4^\circ\text{C}$ for short-term usage (up to 2 weeks) or at -20°C for long-term usage.

Mechanical testing of GelMA and Matrigel hydrogels

50 μL domes of GelMA and Matrigel (Corning, Cat. No. 356231) were added in triplicate to a 24 well-plate (VWR, Cat. No. 734-2325). The GelMA domes were crosslinked

for either 30 s or 1 min, with a light intensity of $8 \text{ mW}/\text{cm}^2$ (365 nm) using benchtop UV-chamber (Veronica DUO, UVD-42). Matrigel domes were solidified by incubating at $+37^\circ\text{C}$, 5% CO_2 for 5 min. Subsequently, the domes were tested with a plunger (surface 0.7 mm^2 ; TA.XTPlus) within a 24 well-plate. A 0.25 mm compression distance with a 0.1 mm/s test speed was used together with a continuous trigger force of 0.0049 N at $+21^\circ\text{C}$ throughout the measurements. The measured force, together with the deformation of the hydrogels, was used to produce a stress-strain curve and to calculate Young's Modulus. The elasticity of the hydrogels was calculated through the compression tests for 20s. The force (Fend; in Newton; N) measured after 20s was divided with the maximum measured force. The calculations were done in Microsoft Excel.

Assessment of cell viability with HCT116 cells

Human colon cancer HCT116 were from ATCC and handled as described previously.³⁶ The cells were cultured in antibiotic-free McCoy 5A media (Cat. No. 392-0420, VWR, Belgium) supplemented with 10% FBS (Cat. No. 11573397, ThermoFisher Scientific, Belgium) and 2 mM Glutamate (Cat. No. 35050061, Gibco) throughout experiments and split every 2–3 days using T25 cell flasks (Cat. No. 10062-872, VWR, Belgium).

For embedding into GelMA, HCT116 cells were seeded at a density of 30,000 cells/well or 300,000 cells/well, respectively, with different GelMA in a U-shaped 96-well plate (Cat. No. 734-2328, VWR, Belgium). Viability of the cells was evaluated with a live-dead staining by using 2 $\mu\text{g}/\text{mL}$ Calcein Green-AM green and 1 $\mu\text{g}/\text{mL}$ propidium iodide (PI), staining live and dead cells, respectively, on days 1 and 4 after embedding. Microscopy of the live-dead stained samples was performed on an inverted widefield fluorescence microscope IX81³⁷ (Olympus-Evident; or PAULA, Leica Microsystems). The counting of live and dead cells was performed with the help of ImageJ software (version 2.14) using following formula (with # = counted

$$\text{cells): Cell viability (\%)} = \left(\frac{\# \text{Calcein green}^+}{\# \text{Calcein green}^+ + \# \text{PI}} \right) \times 100.$$

Intestinal organoids culture

Porcine small intestinal organoids were cultured as described previously.³⁸ Briefly, organoids produced from jejunum crypts isolated from 6 to 7 weeks old female pigs were cultured in growth factor-reduced Matrigel (CorningTM) in antibiotic-free human organoid growth medium (Cat. No. #06010, IntestiCultTM OGM, Stemcell Technologies). For basal-out passaging of organoids, the Matrigel domes were dislodged in a 24-well plate by pipetting for 30–50 times (P10 tip on top of a P1000 pipette tip), depending on the expected size of the organoids. Organoids were then collected in a 15 mL tube, the wells were rinsed

with warm washing media (advanced DMEM F12 supplemented with 10 mM HEPES and 2 mM GlutaMax) and collected in the same 15 mL vial with a final volume of 10 mL, centrifuged (300g, 5 min, 4°C), and kept on ice after removal of the supernatant. Subsequently, organoids were resuspended in ice-cold Matrigel and dispensed to form domes (by 50 μ L per dome) in a pre-warmed flat bottom 24-well plate, solidified and supplemented with 500 μ L of IntestiCult media. The organoids were subcultured every 3–4 days in ratio 1:3 with the approximate density of 100–300 organoids per dome.

Re-embedding of intestinal organoids in GelMA and Matrigel

One day after splitting, two to four of the 50 μ L Matrigel domes with organoids were collected in 12 mL of ice-cold 5 mM EDTA-PBS in 15 mL Lipidure™-pre-coated³⁸ vial and incubated on an orbital shaker platform for 1 h at 4 °C to dissolve the Matrigel. After centrifugation (4°C, 300g, 5 min), the EDTA-PBS solution was carefully removed, and the organoid pellet was gently resuspended in remaining amounts of EDTA-PBS by tapping. Subsequently, organoids were resuspended with Lipidure pre-coated P1000 tips, transferred to a 1.5 mL tube with washing media, centrifuged (21°C, 300g, 5 min), supernatant was removed, and the organoid pellet was placed on ice. Next, organoids were placed within either a 20 or 50 μ L GelMA (prewarmed up to 37°C) or Matrigel domes onto fresh pre-warmed microscopy dish or 24 well-plates, respectively, in IntestiCult media.

Imaging of intestinal organoids

To verify the polarity of the organoids, 20 or 50 μ L Matrigel (Cat. No. 356231, Corning) or GelMA (with or without addition of laminin-111 hydrogel-embedded organoids were fixed with 4% paraformaldehyde (Cat. No. 818708, PFA, Sigma-Aldrich) in PBS (10 min, room temperature), washed with PBS and permeabilised with 0.1% Triton X-100 (Cat. No. T8787, Sigma-Aldrich) in PBS and blocked with 5% FBS/ PBS (30 min, room temperature). The samples were incubated with APN-specific VHH (clone 3L94) fused with the Fc domain of mouse IgG2a (6.7 ng/ μ L in PBS) or with phalloidin labelling reagent for 30 min, washed with PBS, co-stained with 1 μ M Hoechst 33342 and stored overnight protected from light at 4°C. Organoids were imaged on inverted widefield LED-based fluorescence (Olympus IX81, Olympus-Evident)³⁷ or white-light laser-based confocal FLIM (Stellaris 8 Falcon FLIM, Leica microsystems) microscopes, as described previously.³⁶ Briefly, CoolLED pE4000 with 16 channels (365–770 nm) and air objective 40 \times /0.6 UPlanFL N were used on Olympus IX81 microscope, with images converted from .vsi to .tiff and processed with ImageJ (ver.

2.14). For confocal microscopy, HC PL Apo 40 \times /1.25 GLYC corr. objective was used, images were exported from the LAS X software (version 4.6 or higher) and processed with ImageJ software (version 2.14).

For live imaging, organoids embedded in 20 μ L Matrigel or GelMA hydrogel domes, were grown on microscopy dishes (Ibidi) for 3 days (37°C, 5% CO₂). To stain organoids with K⁺-sensitive fluor-ionophore nanoparticles, FI4 nanoparticles³⁹ (10 μ g/mL) were added to the IntestiCult media for overnight incubation prior to the imaging. To visualise lysosomes, LysoSensor Green (4 μ M, Thermo Fisher, Cat. No. L7535) dye was added to the IntestiCult Media for 1 h incubation with organoids. Prior live imaging microscopy analysis the media in wells with domes were exchanged for imaging media (phenol red-free DMEM supplemented with 10 mM HEPES pH 7.2, 1 mM sodium pyruvate, 2 mM GlutaMax, 10 mM D-glucose).³⁶

Statistics

GraphPad (version 10.2) was used for statistical analysis. With the normally distributed data, a Student's *t*-test was used for two groups comparison and two-way ANOVA was performed to compare multiple groups. The standard deviation (SD) was calculated for each condition. If not normally distributed, a Mann-Whitney *U*-test or Kruskal-Wallis tests were used to compare two or multiple groups, respectively. Statistical differences were defined as $p < 0.05$, p -values are represented as * if $p < 0.05$, ** if $p < 0.01$, *** if $p < 0.001$ and **** if $p < 0.0001$. The *N* indicates the number of conditions or samples/organoids used during experiments.

Results and discussion

Laminin-111 influences the mechanical properties of GelMA

To test mechanoreciprocity factors of GelMA hydrogels, we synthesised eight different products, varying in concentration (5% and 10%), molecular weight (90 and 160 kDa) and degree of functionality (DoF, %; 40, 60, and 80). For cell culture experiments, the 50 μ L hydrogel domes were crosslinked for either 30 s or 1 min to prevent overcuring. Mechanical tests showed that the different GelMA conditions exhibited an exponential correlation between 5% and 10% GelMA (90p40, 90p60, 160p60, and 160p80) and their crosslinking time (30 s or 1 min; Figure 1(a)–(f)). The softest hydrogel (5% 90p40, 30 s crosslinked) exhibited a forty-fold Young's Moduli difference compared to the stiffest GelMA (10% 160p80, 1 min crosslinked; that is, 2.45 kPa, vs 101.18 kPa; Supplemental Table S1). The Young's moduli of 5% GelMA crosslinked for 30 s reached range of 2.45–18.08 kPa, while those of

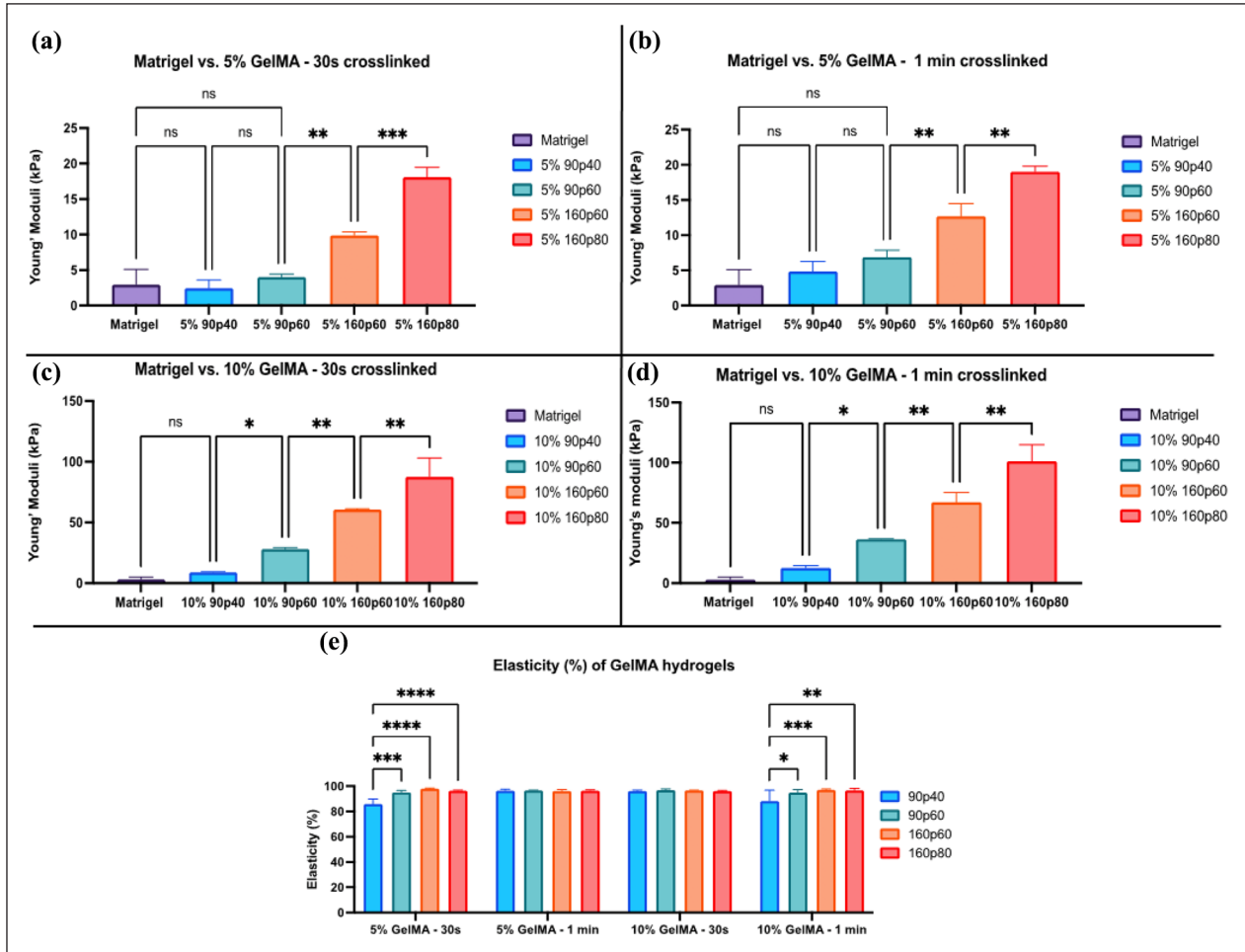


Figure 1. Young's Moduli and elasticity analysis of GelMA hydrogels: (a–d) The effect of the crosslinking time on the Young's moduli in the GelMA hydrogels compared to Matrigel, as a function of GelMA concentration, Mw, DoF, and time. (e) analysis of elasticity of GelMA at different concentrations.

Bars represent the mean with standard deviation. Significant differences are indicated with asterisks (* indicates $p < 0.05$; ** indicates $p < 0.01$; *** indicates $p < 0.001$; **** indicates $p < 0.0001$). $n = 3$ domes per condition. Bars represent the mean with standard deviation.)

10% GelMA were in range of 8.80–87.54 kPa (Figure 1(a)–(d), Supplemental Table S1). Extending the crosslinking time to 1 min resulted in an increase of the Young's moduli of 5% GelMA to 4.84–19.03 kPa and for 10% GelMA to 12.68–101.18 kPa (Supplemental Table S1). However, no significant difference was seen between crosslinking times (Figure 1(e) and (f)). Only the differences in GelMA concentration could result in significant differences between mechanical properties, except for 5% and 10% 90p40 (Supplemental Figure S1A and S1B). With the samples of 5% and 10% 90p40, as well as 5% 90p60 (30s or 1 min crosslinking), we could achieve softness, comparable to Matrigel, that is, 2.94 kPa (Figure 1(a)–(d); Supplemental Table S1). These experiments showed a direct correlation between the mechanical properties of high and low degree methacrylated gelatin and overall consistency in the elastic properties. The tuneability and low batch-to-batch variability of tested X-Pure GelMA

enable to explore the effect of different mechanical properties of this 3D hydrogel, ranging from Matrigel-like and stiffer matrices. This versatility could lead to differences in proliferation, migration, and differentiation of cell cultures.^{23–25} However, when tested with mammalian cultured cells HCT116 (Supplemental Figure S2), we saw that mechanical properties of the different hydrogels do not have an impact on cell death (>90% viability, based on Live-Dead assay). Interestingly, low degree of modification and less stiff GelMA hydrogels displayed formation of spheroids, a phenomenon also observed with Matrigel and other soft hydrogels. Taken together, mechanical property testing underscored the importance of understanding how critical the concentration, MW, DoF, and crosslinking time are for fine-tuning of GelMA. In addition, this ensures consistency and reliability of the hydrogel.

The addition of laminin-111, an important component of the basement membrane (BM), had an overall softening

effect on the different GelMA hydrogels. Addition of 5 $\mu\text{g}/\text{mL}$ laminin-111 still showed significant differences between the Young's moduli of the 5% 160p60 and 160p80 and the 10% 90p60, 160p60, and 160p80 compared to the Matrigel control (Figure 2(a) and (b)). The addition of laminin-111 at 5 $\mu\text{g}/\text{mL}$ resulted in a difference of the Young's modulus of the 5% 90p60 and 160p80 GelMA ranging in 1.80–11.72 kPa, whereas those of 10% GelMA showed 18.72–58.93 kPa (Figure 2(a) and (b); Supplemental Table S2). As expected, addition of laminin-111 at higher concentration (100 $\mu\text{g}/\text{mL}$) resulted in a reduction of stiffness: 5% and 10% 90p40 GelMA hydrogels were excessively soft, making it not possible to accurately measure the hydrogel domes. As such, this condition was excluded from further analysis, in addition to the stiffer 5% and 10% 160p60 conditions. However, we still noticed a significant difference between the Matrigel and the 5% 160p80 and 10% 90p60 and 160p80 conditions (Figure 2(c)–(h)). The supplementation with 100 $\mu\text{g}/\text{mL}$ laminin-111 resulted in the Young's modulus of the 5% 90p60 and 160p80 GelMA hydrogels in range of 1.40–13.23 kPa, whereas those of 10% GelMA showed 10.48–30.95 kPa (Supplemental Table S2). In agreement with the study of Marcinczyk et al.,⁴⁰ a softening effect in the hydrogels was observed with increasing concentration of laminin, even though the effect was non-statistically significant. These experiments confirmed important role of laminin in determining hydrogel mechanical properties.

Embedding of organoids in GelMA hydrogels results in apical-out phenotype

After testing the mechanical properties of the produced GelMA hydrogels, we looked at how they can influence the growth of intestinal organoids. Following the re-embedding procedure, initial light microscopy assessment revealed that the UV-crosslinking conditions (optimised with the human colon cancer HCT116 cells, Supplemental Figure S2) had no apparent effect on the overall cell viability of the intestinal organoids in the various GelMA hydrogels. However, fluorescence microscopy of F-actin labelled organoids (marker of apical membranes),⁴¹ revealed their apical-out polarity topology in GelMA, with the high intensity F-actin labelling at the external side of the organoids (Figure 3). This phenotype was seen throughout all eight tested GelMA types (not shown). Polarity reversion and 'apical-out' phenotype has been previously reported for intestinal organoids deprived from the Matrigel and incubated in low-attachment plates by Amieva and co-workers.^{41,42} Subsequently, this phenotype was reported for organoids and polarised cell lines from other tissues and polymer hydrogels when no ECM cues were present.^{43–46}

Apical-out topology represents an important advance for intestinal organoid engineering, as it enables direct

access of nutrients, pathogens, metabolites, and medium from the apical side of the epithelium. At the same time, such transition results in subsequent lack of stem cell niche-supporting basement membrane, which will result in differentiation of all the crypt-based cells and limited lifespan of the organoid culture. We therefore wondered whether the mechanical properties alone are sufficient to influence basal-out organoid topology. To address this, we tested the effect of different GelMA stiffness and how the addition of laminin-111, a primary component of Matrigel, would influence the topology of embedded organoids (Figure 4). To minimise the number of tested conditions, we chose 90p60 and 160p80 conditions, displaying the most striking differences in mechanical properties.

Analysis of organoids, co-stained with phalloidin and Hoechst 33342 (labelling nuclei) and embedded in 5% and 10% 90p60 and 160p80 GelMA hydrogels, revealed three main morphological types: apical-out, apical-basal, or basal-out (Figure 4(a); Supplemental Figure S4). The apical-out morphology was noted by the F-actin staining outlining the organoids periphery, while the nuclei were localised towards the inner organoid 'body' (Figure 4). Other organoids displayed a double row of cell nuclei, indicating a partial reorganisation of the organoids, resulting in a mixed 'apical-basal' phenotype (Figure 4(b), (c), (g), and (h)). In few organoids, the basal-out phenotype could still be seen in GelMA, where F-actin stained the inside, while nuclei were localised at the organoid periphery. In contrast, Matrigel-embedded organoids demonstrated a full basal-out phenotype after 1 day of re-embedding (Figure 4(k)). Even though the 90p60 GelMA was softer than 160p80 (Supplemental Table S1), the same morphology phenotypes were observed (Supplemental Figure S4). Interestingly, the stiffer 160p80 GelMA displayed a 3D to 2D transition of the intestinal organoids, which was not seen with the 90p60 GelMA hydrogel (Supplemental Figure S3). In all tested GelMA hydrogels, the apical-out and apical-basal morphologies prevailed, suggesting that a stiffer microenvironment did not influence the polarity topology of the intestinal organoids, but positively correlated with observed 3D to 2D transition. Taken together, this data suggests that GelMA hydrogel alone cannot provide the proper microenvironment or biochemical cues for stem cell niche.

Next, we looked if the addition of laminin-111 at concentrations of 5 and 100 $\mu\text{g}/\text{mL}$ (used previously by Dobre, Lutolf and co-workers^{44,47}) could influence the polarity reversion in GelMA. Thus, supplementation of 5 $\mu\text{g}/\text{mL}$ laminin-111 within 5% and 10% 160p80 GelMA did not result in significant differences from the non-supplemented 160p80 GelMA. The laminin-GelMA organoids still showed mostly an apical-out morphology (Figure 4(l) and (m)). However, we also observed the apical-basal morphology after laminin supplementation more frequently, with minor appearance of basal-out

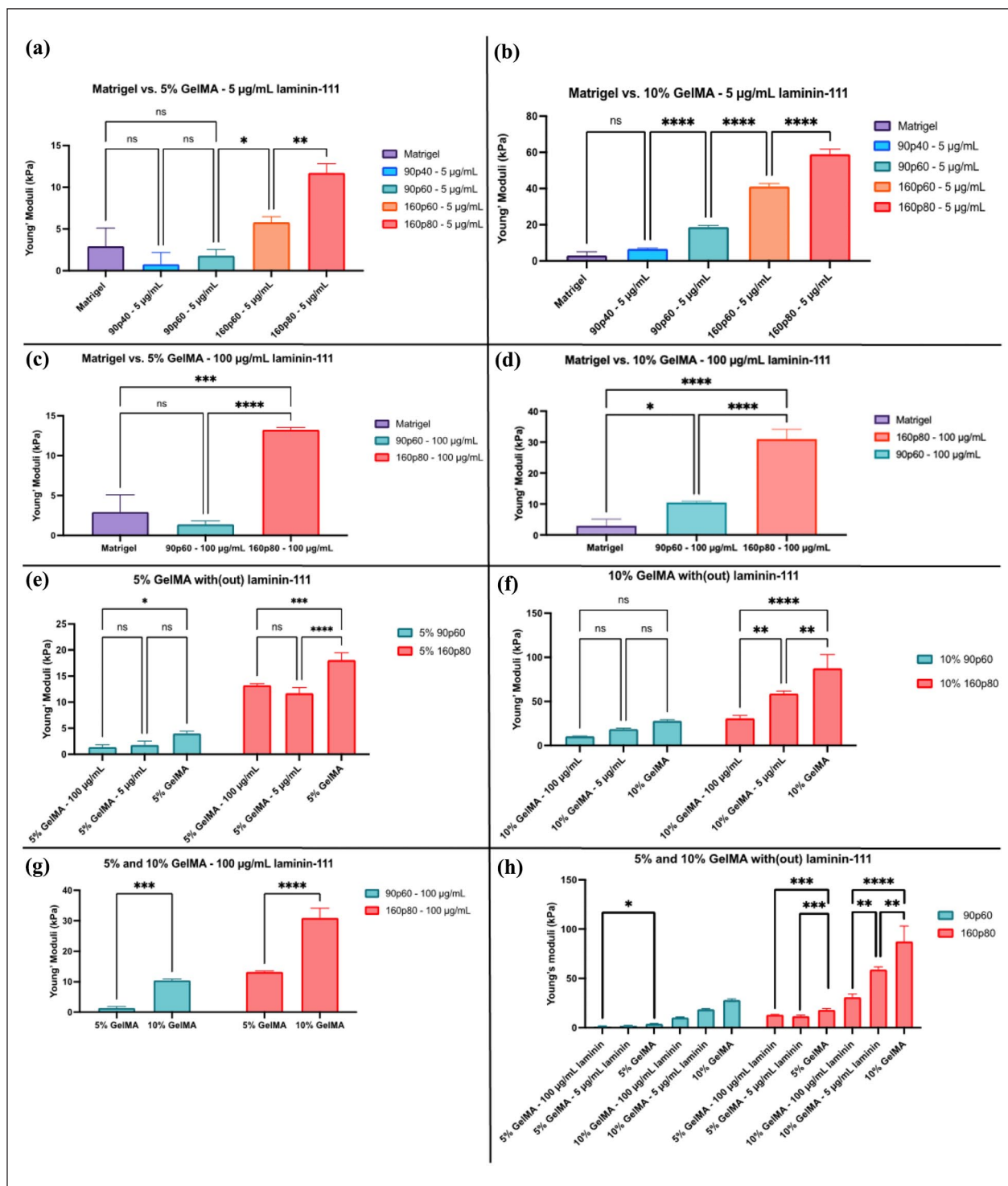


Figure 2. Effect of laminin-111 supplementation on the mechanical properties of GelMA: (a) Young's moduli of the 5% 90p40 and 90p60 GelMA/laminin-111 hydrogels and Matrigel, (b) Young's moduli of the 10% 90p40 GelMA/laminin-111 and Matrigel, (c) Young's moduli of the 5% 90p60 GelMA/laminin-111 and Matrigel, (d) 10% 90p60 and 160p80 GelMA with laminin-111 still display higher Young's moduli than the Matrigel, (e and f) A comparison of all used conditions of the 90p60 and 160p80 GelMA hydrogel, showing a correlation of the stiffness with and without laminin-111 supplementation, (g) The concentration-dependence of the GelMA hydrogels supplemented with 100 µg/mL laminin-111, and (h) An overview of the Young's moduli of 90p60 and 160p80 GelMA tested conditions.

Bars represent the mean with standard deviation. Significant differences are indicated with asterisks (* indicates $p < 0.05$; ** indicates $p < .01$; *** indicates $p < 0.001$; **** indicates $p < 0.0001$). $n = 3$ domes per condition. Bars represent the mean with standard deviation.)

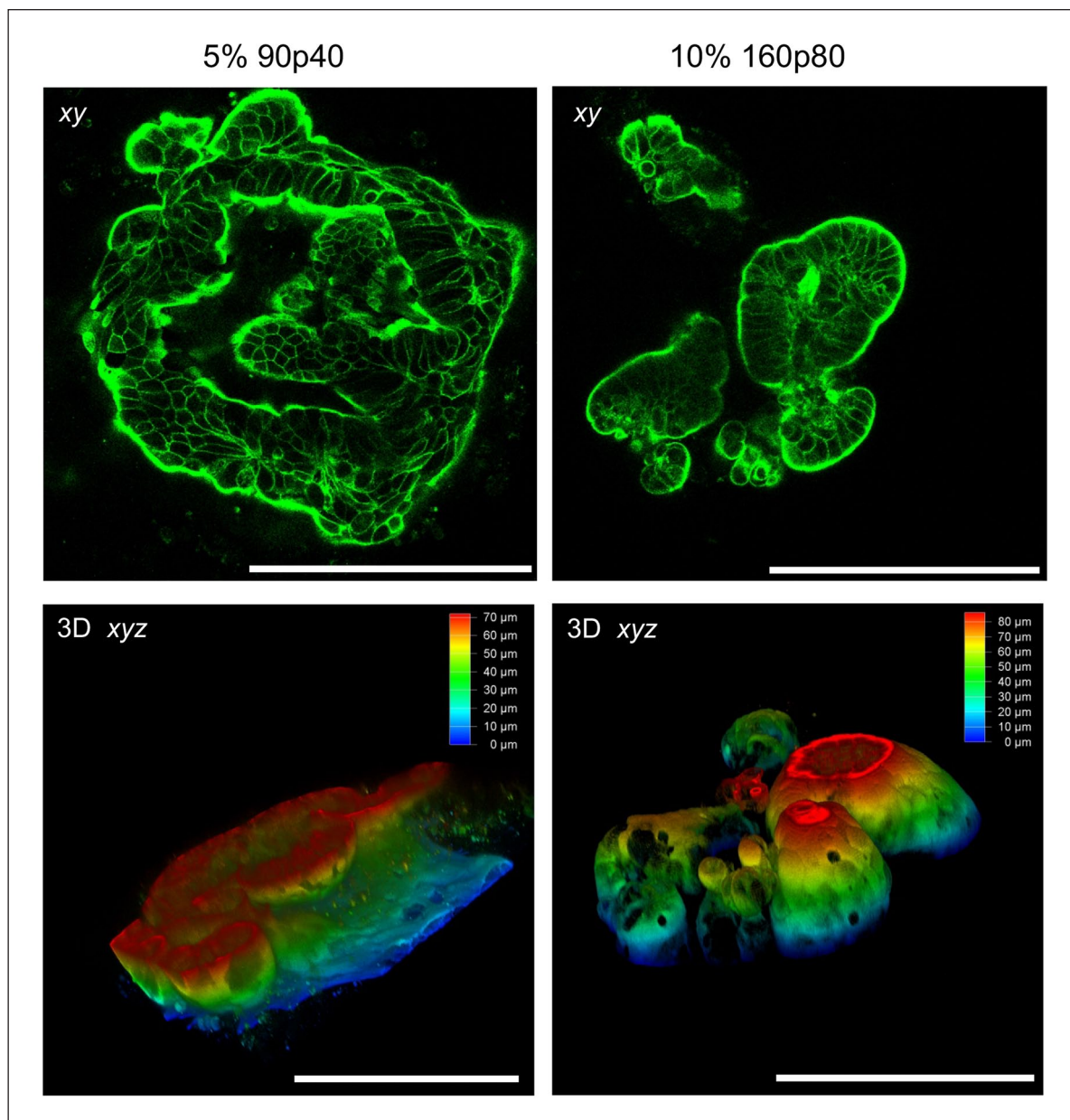


Figure 3. Confocal microscopy reveals polarity reversion and apical-out topology in intestinal organoids embedded in GelMA 2 days after embedding. Organoids were embedded either in 5% 90p40 or 10% 160p80 GelMA, fixed, stained with phalloidin-Alexa Fluor 546 and analysed by confocal microscopy. Top row: Single optical microscopy sections showing peripheral localisation of F-actin. Bottom: depth color-coded 3D reconstructions. Scale bar is 200 μm .

organoids (Figure 4(f), (l), and (m)). We also could see transitioning from 3D to 2D for laminin-supplemented organoids (Supplemental Figures S3 and S4).

We next increased the laminin-111 up to 100 $\mu\text{g}/\text{mL}$ supplementation in 5% and 10% 90p60 GelMA conditions, while keeping the same experimental set-up as with the 160p80 GelMA. Here, a stronger increase of the apical-basal morphology was noted compared, to the non-supplemented conditions, with a slight increase in the

basal-out phenotype of the organoids in the supplemented 90p60 GelMA (Supplemental Figure S4). Although some variability was observed between the experimental replicates, an overall trend of the different morphology types remained consistent (Supplemental Figure S4K and S4L). To validate the widefield fluorescence microscopy data, we performed additional confocal 3D microscopy of organoids embedded in Matrigel and various GelMA conditions and observed the basal-out, apical-basal, and

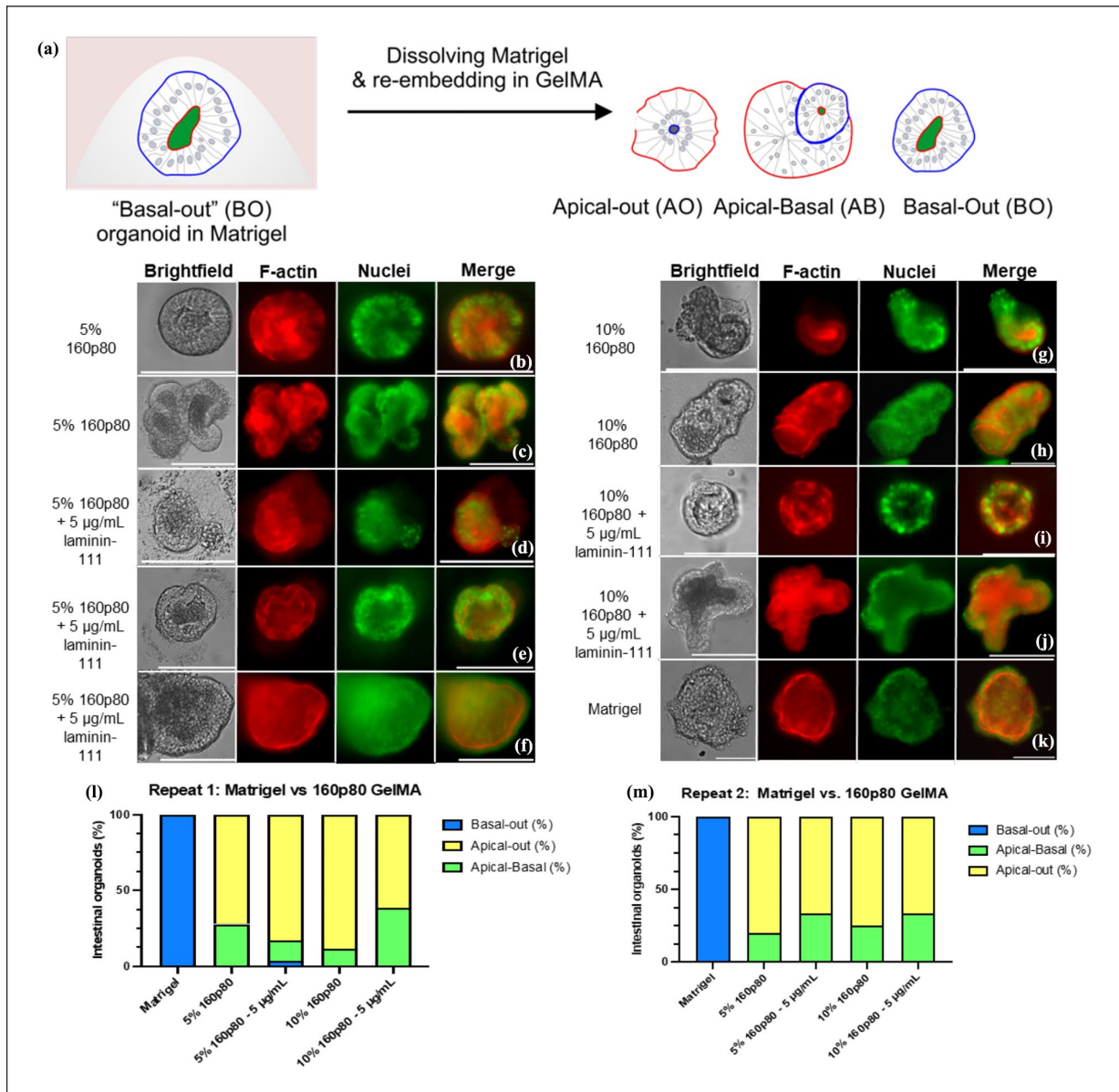


Figure 4. Fluorescence microscopy of intestinal organoids embedded in Matrigel, 160p80 GelMA and with addition of laminin-111. After 1 day of embedding, organoids were fixed, stained with phalloidin (red) and Hoechst 33342 (green) and analysed by widefield fluorescence microscopy: (a) Overview of the apical-out procedure and possible phenotypical outcomes of the embedded organoids, (b–k) An apical-out and apical-basal phenotypes of the organoid embedded 5% and 10% (with or without supplementation of 5 μ g/mL laminin-111) 160p80 GelMA and Matrigel control (basal-out phenotype), and (l and m) calculated frequency of the observed phenotypes within Matrigel and 160p80 GelMA conditions (with or without 5 μ g/mL laminin-111 supplementation). $N = 176$ organoids for all conditions together. Scalebar is 100 μ m.

apical-out phenotypes (Figure 5, Supplemental Figure S5). Taken together, our data suggests that proportional increase of laminin-111 supplementation causes a partial morphology restoration within the GelMA hydrogels. Interestingly, this transition occurred more prominently in the 10% 160p80 supplemented with 5 μ g/mL laminin-111 compared to the softer 10% 160p80 supplemented with 100 μ g/mL laminin-111. Although it might seem contradictory

that stiffness promotes a 3D-to-2D transition, we hypothesise that the higher laminin concentration (100 μ g/mL) reinforces cell-matrix interactions and stabilises the 3D architecture, thus counteracting the effect of lower stiffness. However, the laminin-111 supplementation alone does not suffice to reconstruct the basal membrane, potentially due to the absence of collagen IV, required for stem cells in the intestinal organoids. Additional factors, such as

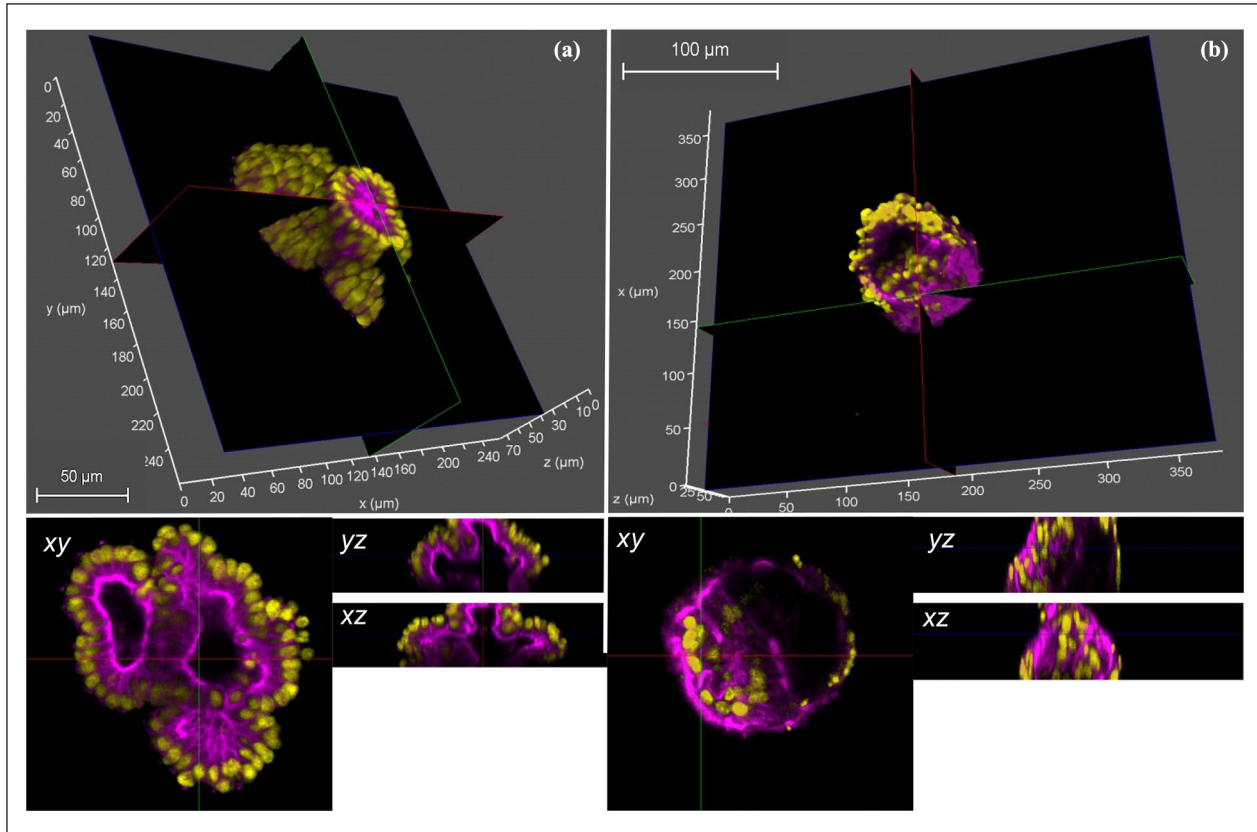


Figure 5. 3D microscopy of the basal-out, apical-basal, and apical-out phenotypes observed with organoids embedded for 2 days in GelMA and Matrigel. Organoids were embedded in hydrogels, fixed, stained with phalloidin-Alexa Fluor 546 (magenta) and Hoechst 33342 (yellow) and analysed by confocal microscopy. XYZ and separate XY, XZ, and YZ sections are shown. (a) Basal-out phenotype observed in Matrigel. (b) Apical-basal organoid, 10% 90p60 GelMA with 100 µg/mL laminin-111. The scale bar is 50 µm (a) and 100 µm (b).

peptides or carbohydrates may be also required to fully support the typical basal-out morphology, growth, and proliferation of the intestinal organoids.

Intestinal organoids demonstrate growth within GelMA independently on the laminin-111 supplementation

Interestingly, we noticed that after embedding, organoids continued to grow in 5% and 10% 90p60 and 160p80 GelMA hydrogels regardless of the supplementation with laminin-111 or their apical-out or basal-out phenotypes, until the day 4 (Figure 6). Thus, 90p60 GelMA with and without laminin-111, showed significant differences between the growth (Figure 6(d)). However, monitoring the growth of embedded organoids after day 4 deemed challenging due to the transition of the organoid culture from a 3D to a 2D monolayer (Supplemental Figure S3; Figure 6), which made accurate measurements of every organoid surface area non-feasible.

We found that organoids re-embedded in 160p80 conditions exhibited an immediate transition from 3D to 2D by

day 2, which prohibited any accurate surface area measurements (Figure 6(b)). Only one condition (10% 160p80 with 100 µg/mL laminin-111) did not show such transition. In comparison with a Matrigel (which demonstrates rapid growth and requires a splitting every 2–3 days to prevent overgrowth), growth in GelMA was slower. After 1 week of culturing GelMA organoids died (not shown).

Physiological relevance of the apical-out transition in GelMA

Observed the apical-out, as well as partial reversal to basal-out polarity of organoids in GelMA represents an attractive feature for recapitulating biomolecular interactions of organoids from the apical side or comparing these interactions between apical and basal membranes. Using GelMA for producing apical-out organoid culture has also advantages of (i) continued organoid growth and (ii) potential application of tuneable mechanical properties of the hydrogels (with or without laminin), which can help better mimicking mucus and host-microbe interactions at the apical membrane occurring *in vivo*.^{48–50} We therefore

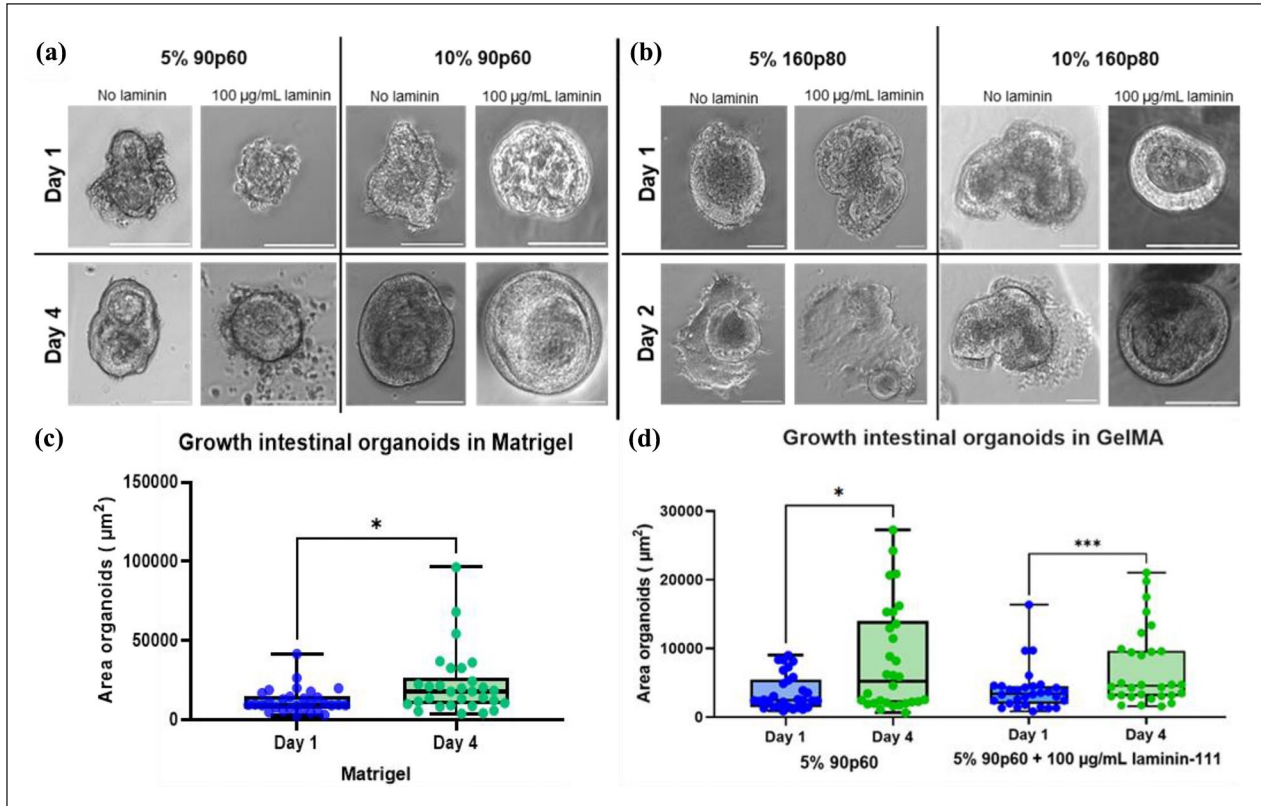


Figure 6. Growth of organoids in Matrigel, 5% and 10% 90p60 and 160p80 GelMA hydrogels on day 1 and day 4 after embedding: (a) Comparison of intestinal organoid growth in 5% and 10% 90p60 between day 1 and day 4. Scalebar is 100 µm, (b) comparison of intestinal organoid growth in 5% and 10% 160p80 between day 1 and day 2. The transitioning of the 3D to 2D pattern was noted in three of four conditions, together with some growth. Scalebar is 100 µm, (c) growth of organoids embedded within Matrigel on day 1 and day 4, and (d) growth patterns of organoids on day 1 and day 4 in 5% 90p60 without laminin-111 and with laminin-111. $N=30$ organoids per condition. Each dot represents the area (μm^2) of the measured organoids per conditions. *indicates $p < 0.05$; *** indicates $p < 0.001$.

tested if GelMA organoids (1 day after embedding) showed comparable properties to conventional Matrigel-embedded cultures. Ion homeostasis and pH are important for intestinal tissue function.^{51,52} Using K^+ -sensitive nanosensor FI4,^{39,53} we compared staining of Matrigel- and GelMA-embedded organoids using fluorescence microscopy and FLIM^{54,55} (Supplemental Figure S6). Since with the basal-out Matrigel-embedded organoids FI4 displayed basal-membrane and luminal staining, it was difficult to compare its localisation in the apical-out organoids. However, when we looked at the distribution of fluorescence lifetimes, we found them comparable, in both types of organoids. This suggests that FI4 shows localisation in the same cell types and with similar efficiency in both apical and basal-out organoids. To look at pH homeostasis, we stained organoids with LysoSensor Green dye, which labels different types of endosomes and lysosomes and displays pH-dependent fluorescence lifetime changes.⁵⁶ Data shown on Supplemental Figure S7 confirmed that despite drastic differences in topology, both GelMA and Matrigel-embedded

organoids displayed similar dynamics of fluorescence lifetimes/pH in endo- and lysosomal compartments.

We confirmed apical-out topology using F-actin labelling (Figures 3 and 4). However, we could not rule out the possibility that observed topology could be also a result of actin cytoskeleton reorganisation within the cells, rather than ‘true’ reversion of the apical- and basolateral membranes in the organoids during the embedding.⁵⁷ To better understand this, we also performed immunofluorescence labelling of organoids with the marker of apical membranes, aminopeptidase N (APN), characteristic marker for intestine, kidney, and liver tissues.⁵⁸ Confocal microscopy of APN- and F-actin labelling in Matrigel and GelMA-embedded organoids confirmed co-localisation of these two markers of the apical membranes and the observed apical-out transition (Figure 7). Anti-APN antibody showed brighter staining of the apical membranes, predominantly localised at the internal, luminal side of the Matrigel-embedded organoids and at the external membranes in 90p60 GelMA-embedded organoids, even in the

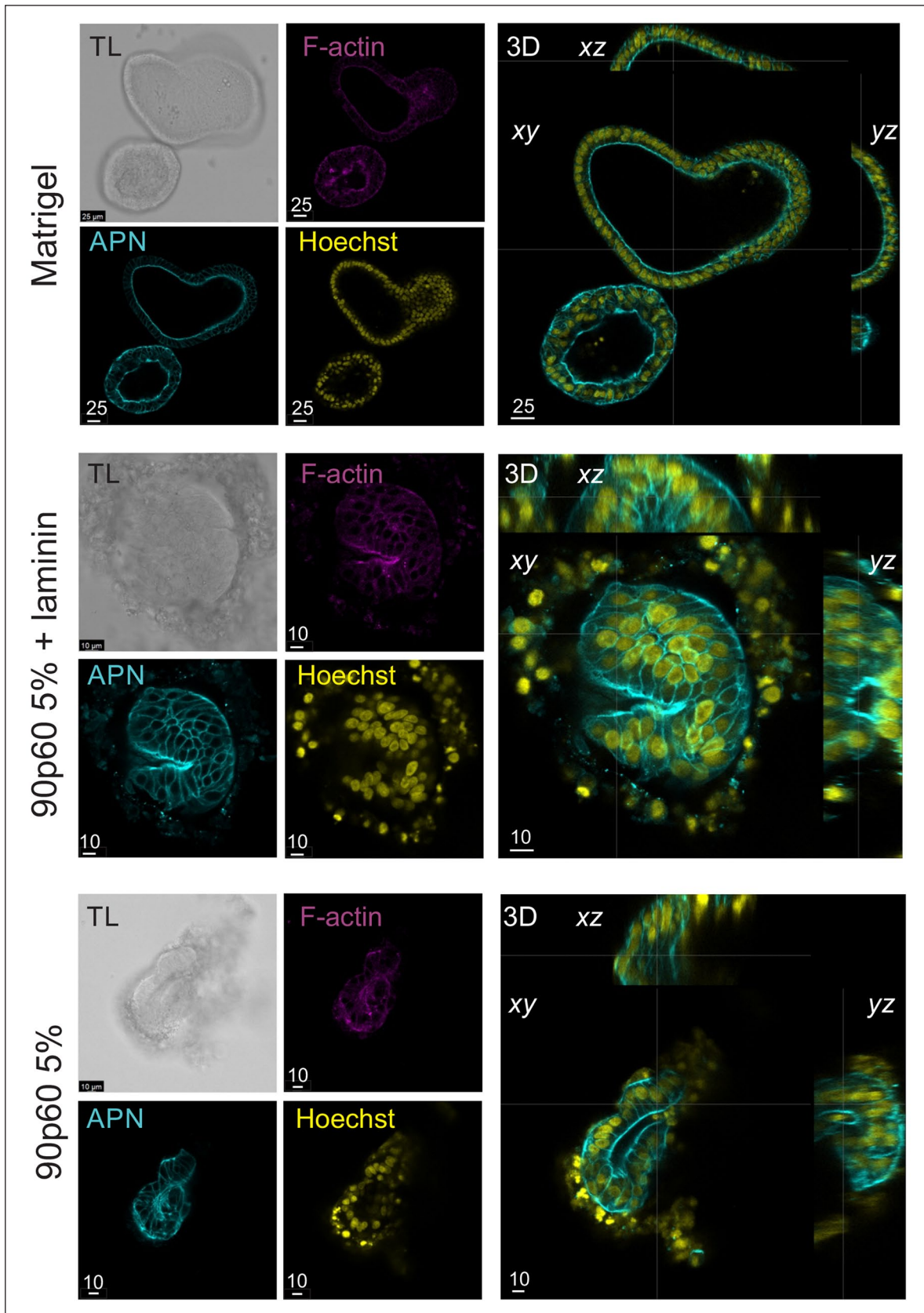


Figure 7. Confocal microscopy of fixed and phalloidin-Texas Red and anti-APN antibody-stained organoids, 1 day after embedding either in Matrigel, 90p60 5% or 90p60 5%, 100 $\mu\text{g}/\text{mL}$ laminin GelMA. Transmission light (TL), Phalloidin (magenta), APN (cyan), and Hoechst 33342 (yellow) fluorescence images (single optical sections) are shown. Right: slice 3D views of the organoids. Scale bar is in μm .

presence of laminin-111. This was also confirmed with 160p80 GelMA organoids (not shown).

Conclusion

Here, we thoroughly studied mechanical properties and crosslinking conditions for different GelMA hydrogels, with respect of their applicability for the culture of stem cell-derived intestinal organoids. GelMA showed excellent biocompatibility with cultured colon cancer cells. However, encapsulation of organoids in GelMA with Young's moduli ranging from 2.4 to 101 kPa (also covering the compressive modulus of Matrigel) resulted in polarity reversion and yielding apical-out organoids, irrespectively to the stiffness of hydrogels. This means that GelMA alone is not sufficient to recapitulate basal membrane components, present in widely used Matrigel. This was confirmed by supplementing GelMA hydrogels with laminin-111, which led to partial restoration of 'normal' basal-out topology and resulting in apical-basal organoids. Interestingly, we found that stiffer gels resulted in 3D to 2D transition of organoids and that organoids could continue to grow in GelMA, with and without laminin-111, though for a very limited time. We confirmed the viability and topology of apical-out organoids using staining with nano- and dye-based sensors, as well as with the apical membrane markers.

In addition to the mechanical cues, GelMA can hypothetically still provide 'biochemical' cell-interacting factors even in the absence of laminin-111, therefore affecting the observed polarity reversion phenomenon. However, the most plausible explanation is that it provides only the mechanical cues, as the polarity reversion was also reported before within fully synthetic hydrogels lacking any biochemical signalling, or in the absence of Matrigel.^{38,41,43,46} In addition, polarity reversion was observed in all tested GelMA conditions, independently from the Mw and DoF, supporting that the lack of correct biochemical signalling at the basal membrane is the main contributing factor for the observed phenomenon.

Collectively, our experiments demonstrate that GelMA represents an attractive biomaterial with tuneable properties, promising for intestinal organoids applications, where apical membrane access and controlled polarity is essential, that is, in organ-on-a-chip, host-microbe and related tissue engineering applications.

Acknowledgements

We thank Hang Zhou and Simone Perottoni for help with organoid cultures and Jan-Philip Zegwaart with initial guidance with the project.

ORCID iDs

Lenie Vanhove  <https://orcid.org/0009-0006-5402-4683>
 Ruslan I. Dmitriev  <https://orcid.org/0000-0002-0347-8718>
 Irina A. Okkelman  <https://orcid.org/0000-0002-7014-6887>

Author contributions

LV: methodology, experimental design, and drafting the manuscript. TVG, RVDM, and BD: resources, methodology, and drafting the manuscript. IAO and RID: conceiving the study, supervision, experimental design, methodology, and drafting the manuscript. The manuscript was written through contributions of all authors. All authors have given approval to the final version of the manuscript.

Funding

The author(s) disclosed receipt of the following financial support for the research, authorship, and/or publication of this article: This work was supported by the Special Research Fund (BOF) grants (BOF/STA/202009/003, BOF/BAF/1y/25/1/004), Research Foundation Flanders (FWO, I001922N, I004124N), and the European Union, fliMAGIN3D-DN Horizon Europe-MSCA-DN No. 101073507 grants.

Declaration of conflicting interests

The author(s) declared the following potential conflicts of interest with respect to the research, authorship, and/or publication of this article: TVG and RVDM are employees of Rousselot BV. Other authors do not have any conflict of interest.

Supplemental material

Supplemental material for this article is available online.

References

1. Rahmani S, Breyner NM, Su H-M, et al. Intestinal organoids: a new paradigm for engineering intestinal epithelium in vitro. *Biomaterials* 2019; 194: 195–214.
2. Yin X, Mead BE, Safaee H, et al. Stem cell organoid engineering. *Cell Stem Cell* 2016; 18: 25.
3. Kane KI, Lucumi Moreno E, Lehr CM, et al. Determination of the rheological properties of Matrigel for optimum seeding conditions in microfluidic cell cultures. *AIP Adv* 2018; 8: 125332.
4. Sato T, Vries RG, Snippert HJ, et al. Single Lgr5 stem cells build crypt-villus structures in vitro without a mesenchymal niche. *Nature* 2009; 459: 262–265.
5. Moerkens R, Mooiweer J, Ramírez-Sánchez AD, et al. An iPSC-derived small intestine-on-chip with self-organizing epithelial, mesenchymal, and neural cells. *Cell Rep* 2024; 43: 114247.
6. Xiang T, Wang J and Li H. Current applications of intestinal organoids: a review. *Stem Cell Res Ther* 2024; 15: 155.
7. Yang Y, Cui J, Kong Y, et al. Organoids: new frontiers in tumor immune microenvironment research. *Front Immunol* 2024; 15: 1422031.
8. Cea C, Zhao Z, Wisniewski DJ, et al. Integrated internal ion-gated organic electrochemical transistors for stand-alone conformable bioelectronics. *Nat Mater* 2023; 22: 1227–1235.
9. Kim S, Min S, Choi YS, et al. Tissue extracellular matrix hydrogels as alternatives to Matrigel for culturing gastrointestinal organoids. *Nat Commun* 2022; 13: 1692.
10. Chang N, He J, Guo Y, et al. Effects of Matrigel on growth and development of cerebral organoids. *Mater Express* 2022; 12: 616–627.

11. Kleinman HK, Kim K and Kang H. Matrigel uses in cell biology and for the identification of thymosin β_4 , a mediator of tissue regeneration. *Appl Biol Chem* 2018; 61: 703–708.
12. Reed J, Walczak WJ, Petzold ON, et al. In situ mechanical interferometry of Matrigel films. *Langmuir* 2009; 25: 36–39.
13. Benton G, Arnaoutova I, George J, et al. Matrigel: from discovery and ECM mimicry to assays and models for cancer research. *Adv Drug Deliv Rev* 2014; 79: 3–18.
14. Kaur S, Kaur I, Rawal P, et al. Non-Matrigel scaffolds for organoid cultures. *Cancer Lett* 2021; 504: 58–66.
15. Kleinman HK and Martin GR. Matrigel: basement membrane matrix with biological activity. *Semin Cancer Biol* 2005; 15(5): 378–386.
16. Kozlowski MT, Crook CJ and Ku HT. Towards organoid culture without Matrigel. *Commun Biol* 2021; 4: 1387.
17. Gan Z, Qin X, Liu H, et al. Recent advances in defined hydrogels in organoid research. *Bioact Mater* 2023; 28: 386–401.
18. Hushka EA, Blatchley MR, Macdougall LJ, et al. Fully synthetic hydrogels promote robust crypt formation in intestinal organoids. *bioRxiv* 2024: 2024.2007.2006.602364. DOI: 10.1101/2024.07.06.602364.
19. Hushka EA, Yavitt FM, Brown TE, et al. Relaxation of extracellular matrix forces directs crypt formation and architecture in intestinal organoids. *Adv Healthc Mater* 2020; 9: 1901214.
20. Rezakhani S, Gjorevski N and Lutolf M. Extracellular matrix requirements for gastrointestinal organoid cultures. *Biomaterials* 2021; 276: 121020.
21. Van Den Bulcke AI, Bogdanov B, De Rooze N, et al. Structural and rheological properties of methacrylamide modified gelatin hydrogels. *Biomacromolecules* 2000; 1: 31–38.
22. Ribezzi D, Zegwaart J-P, Van Gansbeke T, et al. Multi-material volumetric bioprinting and plug-and-play suspension bath biofabrication via bioresin molecular weight tuning and via multiwavelength alignment optics. *Adv Mater* 2025; 37: e2409355.
23. Lavrentieva A, Fleischhammer T, Enders A, et al. Fabrication of stiffness gradients of GelMA hydrogels using a 3D printed micromixer. *Macromol Biosci* 2020; 20: 2000107.
24. van Bochove B and Grijpma DW. Photo-crosslinked synthetic biodegradable polymer networks for biomedical applications. *J Biomater Sci Polym Ed* 2019; 30: 77–106.
25. Narang P, Raju B, Jumah F, et al. The evolution of 3D anatomical models: a brief historical overview. *World Neurosurg* 2021; 155: 135–143.
26. Yue K, Trujillo-de Santiago G, Alvarez MM, et al. Synthesis, properties, and biomedical applications of gelatin methacryloyl (GelMA) hydrogels. *Biomaterials* 2015; 73: 254–271.
27. Aisenbrey EA and Murphy WL. Synthetic alternatives to Matrigel. *Nat Rev Mater* 2020; 5: 539–551.
28. Bupphathong S, Quiroz C, Huang W, et al. Gelatin methacrylate hydrogel for tissue engineering applications—a review on material modifications. *Pharmaceuticals* 2022; 15: 171.
29. Vasudevan J, Lim CT and Fernandez JG. Cell migration and breast cancer metastasis in biomimetic extracellular matrices with independently tunable stiffness. *Adv Funct Mater* 2020; 30: 2005383.
30. Zhang J, Liu C, Li X, et al. Application of photo-crosslinkable gelatin methacryloyl in wound healing. *Front Bioeng Biotechnol* 2023; 11: 1303709.
31. Carpentier N, Ye S, Delemarre MD, et al. Gelatin-based hybrid hydrogels as matrices for organoid culture. *Biomacromolecules* 2024; 25: 590–604.
32. Kjar A, Haschert MR, Zepeda JC, et al. Biofunctionalized gelatin hydrogels support development and maturation of iPSC-derived cortical organoids. *Cell Rep* 2024; 43: 114874.
33. Qian J, Lu E, Xiang H, et al. GelMA loaded with exosomes from human minor salivary gland organoids enhances wound healing by inducing macrophage polarization. *J Nanobiotechnol* 2024; 22: 550.
34. Jee JH, Lee DH, Ko J, et al. Development of collagen-based 3D matrix for gastrointestinal tract-derived organoid culture. *Stem Cells Int* 2019; 2019: 8472712.
35. Bakshi S, Sanz Garcia R, Van der Weken H, et al. Evaluating single-domain antibodies as carriers for targeted vaccine delivery to the small intestinal epithelium. *J Control Release* 2020; 321: 416–429.
36. Debruyne AC, Okkelman IA, Heymans N, et al. Live microscopy of multicellular spheroids with the multimodal near-infrared nanoparticles reveals differences in oxygenation gradients. *ACS nano* 2024; 18: 12168–12186.
37. Okkelman I, Verduyck C, Kondrashina AV, et al. Affordable oxygen microscopy-assisted biofabrication of multicellular spheroids. *J Vis Exp* 2022; 182: e63403. DOI:10.3791/63403.
38. Okkelman IA, Zhou H, Borisov SM, et al. Fluorescence Lifetime Imaging Microscopy (FLIM) visualizes internalization and biological impact of nanoplastics in live intestinal organoids. *bioRxiv* 2025: 2025.2001.2027.635069. DOI: 10.1101/2025.01.27.635069.
39. Müller BJ, Zhdanov AV, Borisov SM, et al. Nanoparticle-based fluoroionophore for analysis of potassium ion dynamics in 3D tissue models and in vivo. *Adv Funct Mater* 2018; 28: 1704598.
40. Marcinczyk M, Elmashady H, Talovic M, et al. Laminin-111 enriched fibrin hydrogels for skeletal muscle regeneration. *Biomaterials* 2017; 141: 233–242.
41. Co JY, Margalef-Català M, Monack DM, et al. Controlling the polarity of human gastrointestinal organoids to investigate epithelial biology and infectious diseases. *Nat Protoc* 2021; 16: 5171–5192.
42. Margalef-Català M, Li X, Mah AT, et al. Controlling epithelial polarity: a human enteroid model for host-pathogen interactions. *Cell Rep* 2019; 26: 2509–2520.e4.
43. Chen W, Yao Q, Wang R, et al. Highly efficient methods to culture mouse cholangiocytes and small intestine organoids. *Front Microbiol* 2022; 13: 907901.
44. Dobre O, Oliva MA, Ciccone G, et al. A hydrogel platform that incorporates laminin isoforms for efficient presentation of growth factors—neural growth and osteogenesis. *Adv Funct Mater* 2021; 31: 2010225.
45. Patricio D, Santiago J, Mano JF, et al. Organoids of the male reproductive system: challenges, opportunities, and their

- potential use in fertility research. *WIREs Mech Dis* 2023; 15: e1590.
46. Vanhoeijen R, Okkelman IA, Rogier N, et al. Poly(2-alkyl-2-oxazoline) hydrogels as synthetic matrices for multicellular spheroid and intestinal organoid cultures. *Biomacromolecules* 2025; 26(3): 1860–1872.
 47. Gjorevski N, Sachs N, Manfrin A, et al. Designer matrices for intestinal stem cell and organoid culture. *Nature* 2016; 539: 560–564.
 48. Bansil R, Stanley E and LaMont JT. Mucin biophysics. *Annu Rev Physiol* 1995; 57: 635–657.
 49. Snyder J, Wang C-M, Zhang AQ, et al. Materials and micro-environments for engineering the intestinal epithelium. *Ann Biomed Eng* 2020; 48: 1916–1940.
 50. Wang Y, Gunasekara DB, Reed MI, et al. A microengineered collagen scaffold for generating a polarized crypt-villus architecture of human small intestinal epithelium. *Biomaterials* 2017; 128: 44–55.
 51. Kiela PR and Ghishan FK. Ion transport in the intestine. *Curr Opin Gastroenterol* 2009; 25: 87–91.
 52. Liu Y, Reyes E, Castillo-Azofeifa D, et al. Intracellular pH dynamics regulates intestinal stem cell lineage specification. *Nat Commun* 2023; 14: 3745.
 53. Müller BJ, Borisov SM and Klimant I. Red-to NIR-emitting, BODIPY-based, K⁺-selective fluoroionophores and sensing materials. *Adv Funct Mater* 2016; 26: 7697–7707.
 54. Barroso M, Monaghan MG, Niesner R, et al. Probing organoid metabolism using fluorescence lifetime imaging microscopy (FLIM): the next frontier of drug discovery and disease understanding. *Adv Drug Deliv Rev* 2023; 201: 115081.
 55. Dmitriev RI, Intes X and Barroso MM. Luminescence lifetime imaging of three-dimensional biological objects. *J Cell Sci* 2021; 134: 1–17.
 56. Deng D, Wang B, Guan Y, et al. Quantitative profiling of lysosomal pH heterogeneity using fluorescence lifetime imaging microscopy. *bioRxiv* 2023: 2023.2009.2025.559395.
 57. Miyoshi J and Takai Y. Structural and functional associations of apical junctions with cytoskeleton. *Biochim Biophys Acta (BBA) Biomembr* 2008; 1778: 670–691.
 58. Moore BD, Jin RU, Osaki L, et al. Identification of alanyl aminopeptidase (CD13) as a surface marker for isolation of mature gastric zymogenic chief cells. *Am J Physiol Gastrointest Liver Physiol* 2015; 309: G955–G964.